Nonlinear Dyn (2007) 50:387–408
DOI 10.1007/s11071-006-9183-0

ORIGINAL ARTICLE

Time and frequency domain nonlinear system characterization for mechanical fault identification

Muhammad Haroon · Douglas E. Adams

Received: 31 May 2006 / Accepted: 27 June 2006 / Published online: 20 January 2007

Abstract Mechanical systems are often nonlinear with nonlinear components and nonlinear connections, and mechanical damage frequently causes changes in the nonlinear characteristics of mechanical systems, e.g. loosening of bolts increases Coulomb friction nonlinearity. Consequently, methods which characterize the nonlinear behavior of mechanical systems are well-suited to detect such damage. This paper presents passive time and frequency domain methods that exploit the changes in the nonlinear behavior of a mechanical system to identify damage.

In the time domain, fundamental mechanics models are used to generate restoring forces, which characterize the nonlinear nature of internal forces in system components under loading. The onset of nonlinear damage results in changes to the restoring forces, which can be used as indicators of damage. Analogously, in the frequency domain, transmissibility (output-only) versions of auto-regressive exogenous input (ARX) models are used to locate and characterize the degree to which faults change the nonlinear correlations present in the response data. First, it is shown that damage causes changes in the restoring force characteristics, which can be used to detect damage. Second, it is shown that damage also alters the nonlinear correlations in the data that can be used to locate and track the progress of damage. Both restoring forces and auto-regressive transmissibility methods utilize operational response data for damage identification. Mechanical faults in ground vehicle suspension systems, e.g. loosening of bolts, are identified using experimental data.

Keywords Damage identification · Discrete frequency models · Force-state maps · Restoring force · Nonlinear characterization · Nonlinear frequency domain ARX models

Abbreviations

ARX	Auto-regressive exogenous
DFM	Discrete frequency model
FRF	Frequency response function
OEM	Original equipment manufacturer

1 Introduction

Mechanical systems are often nonlinear as a result of nonlinearities in the material properties and the components. Additionally, the components are interconnected through nonlinear connections, e.g., bolts, welds and bushes. These connections lead to nonlinear behavior of the components and nonlinear interactions within the system. Mechanical damage often causes changes in the nonlinear behavior, e.g. loosening of bolts increases Coulomb friction nonlinearity, or even introduces nonlinearity. Consequently, methods that

M. Haroon · D. E. Adams (✉)
Ray W. Herrick Laboratories, School of Mechanical Engineering, Purdue University, 140 S. Intramural Drive, West Lafayette, IN 47907-2031, USA
e-mail: deadams@purdue.edu

characterize the nonlinear behavior of systems are well-suited for nonlinear mechanical damage identification.

Characterization of nonlinear vibrating systems is a well-researched area with a significant amount of literature and techniques available. Some techniques are based on frequency modulation, such as frequency deconvolution [1], Hilbert transforms [2, 3] and wavelet transforms [4]. These techniques utilize changes in system natural frequencies with changes in response amplitude for nonlinear characterization. In addition, Leontaritis and Billings [5] have used correlation functions in time to characterize nonlinear systems. Storer and Tomlinson [6] used higher order frequency response functions to characterize nonlinear structural dynamic systems. Collis et al. [7] have also used higher order spectra, bispectra and trispectra, to characterize nonlinearities. Surace et al. [8] used the restoring force method to characterize the nonlinear nature of automotive shock absorbers and Audenino and Belingardi [9] also recognized the merit of this method. Haroon et al. [10, 11] used restoring forces to characterize the nonlinearities as part of a system identification methodology in the absence of external input measurements. McGee et al. [12] used drops in the ordinary spectral coherence functions associated with nonlinear frequency permutations to characterize the nonlinearities in tire-vehicle suspension systems in the absence of an input measurement. Adams and Allemang [13] used discrete frequency models [14] to derive an experimental frequency domain nonlinear indicator function. Unlike ordinary spectral coherence functions, which only indicate input–output relations at a single frequency, these functions relate the error at each frequency to errors at frequencies across the band of interest. This enables the technique to distinguish between system nonlinearities and bias errors localized in frequency.

This paper presents two nonlinear damage identification techniques that utilize passive response data along with fundamental mechanics models to interrogate the nonlinear behavior of a vehicle suspension system. The first one is the restoring force method, which has its origins in the work by Masri et al. [15–18], who used recursive least squares for linear parameter identification and a nonparametric method for expressing the nonlinear characteristics (force-state maps) in terms of orthogonal functions. Surace et al. [8] used it to characterize the dynamic properties of automotive dampers and Haroon et al. [10, 11] extended the technique to nonlinear characterization and system identification of mechanical systems in the absence of an input measurement. The authors highlighted a valuable feature of restoring forces; only response acceleration measurements are needed to generate restoring force curves, which is important for applying them to operating data. Here, restoring forces are used to characterize the nonlinear internal loads of the components of a mechanical system in terms of frequency and then changes in the restoring forces with the onset and progression of damage are used for damage detection.

The second method is based on the Discrete Frequency Domain Models presented by Adams and Allemang [14]. Adams [19] used these models to develop frequency domain auto-regressive exogenous input (ARX) models, which relate the frequency response of a nonlinear system at each frequency to the input and output spectra within a given frequency band. These harmonic relationships indicate that the response of a nonlinear vibrating system at a particular frequency, ω_k, $X(\omega_k)$, is correlated with both the input(s) at that frequency, $F(\omega_k)$, and the response at sub and super-harmonics of that frequency, $X(\omega_{k-i})$ and $X(\omega_{k+i})$. Adams and Farrar [20] applied frequency domain ARX models to damage identification by developing features that can be used to detect changes in the nonlinear behavior of structural systems with the onset of damage. Similar models are used here to detect and follow the progress of damage in a mechanical system. When the transmissibility version of the ARX models is used, they can help to detect and locate damage. The reason for this dual capability is that transmissibility functions contain only the transmission zeros of the system and, hence, are more sensitive to local changes in system characteristics [21, 22].

In the following sections, the techniques described above are explained in more detail and then used to identify simulated damage in ground vehicle suspension systems.

2 Fault identification methods

2.1 Restoring forces

The restoring force is an internal force that opposes the motion of an inertial element within a system, e.g., the left-hand side of Newton's Second Law for a body with constant mass, m, and acceleration vector, $\mathbf{a}$: $\sum \mathbf{F} = m\mathbf{a}$. The local stiffness and damping in a

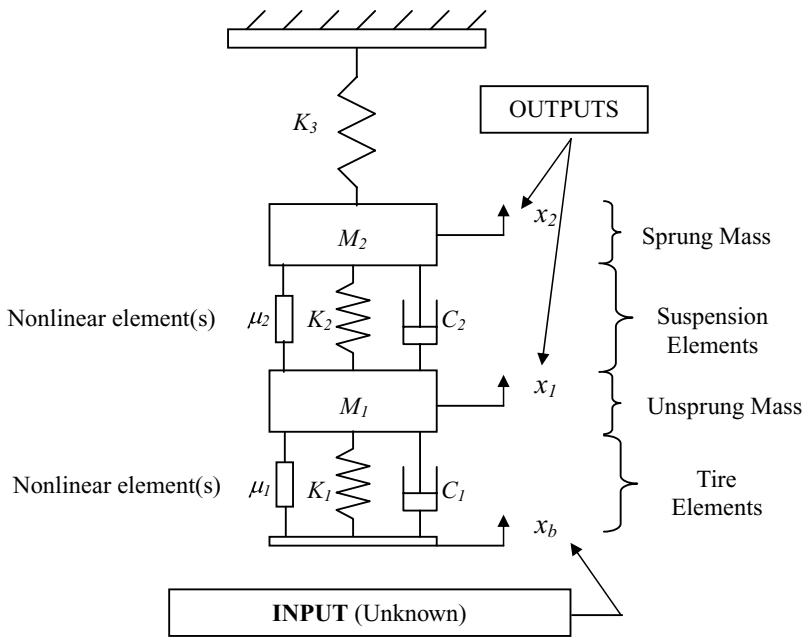

Fig. 1 Quarter car model

mechanical system resist the motion of a given inertia; consequently, the forces in the stiffness and damping elements are referred to as components of the restoring forces. Individual nonlinearities have particular restoring forces; therefore, the nonlinear nature of the internal forces can be characterized by the restoring forces within a system.

An advantage of the restoring force technique is that it only requires that the output accelerations of a system be measured. Consider the two degree-of-freedom quarter car model shown in Fig. 1. The equation of motion for the sprung mass, M_2, provides the following expression for the restoring force in the suspension:

$$M_2\ddot{x}_2 = -C_2(\dot{x}_2 - \dot{x}_1) - K_2(x_2 - x_1) - K_3x_2 + N_1[x_1(t), x_2(t), \dot{x}_1(t), \dot{x}_2(t)] \quad (1)$$

where $x_k(t)$ are the displacements of the unsprung and sprung masses, M_k, C_2 is the suspension damping, K_k are stiffness in the suspension and vehicle body and $N_1[x_1(t), x_2(t), \dot{x}_1(t)\dot{x}_2(t)]$ denotes the nonlinear forces in the suspension. The body stiffness to ground accounts for the resistance supplied by the inertia of the vehicle to the motion of a vehicle corner.

The plots between the acceleration of the sprung mass and the relative velocity or the relative displacement between the sprung mass and the unsprung mass allow the damping or stiffness restoring force, respectively, in the suspension to be estimated. Figure 2 shows the plots of the damping restoring force regression for a particular input amplitude and frequency showing the nature of the damping nonlinearities observed in the strut of a suspension system of an experimental vehicle test bed. The frequency characteristics of the internal forces can be observed by plotting the restoring forces at different frequencies. Restoring force plots can be generated for any two response locations by using similar two degree-of-freedom models.

The main features of restoring forces that make them suitable for nonlinear damage detection are,

(1) Restoring forces are determined by the damping and stiffness (linear or nonlinear) of a system. Structural damage often causes changes in these system parameters and, consequently, the restoring forces.
(2) Individual nonlinearities have distinct restoring forces and damage often causes changes in the nonlinear characteristics, which can be indictors of damage.

The frequency dependent nature of restoring forces dictates that the inputs should be narrowband so that the characteristics, and changes in those characteristics, can be observed at particular discrete frequencies. Acceleration measurements are the most convenient

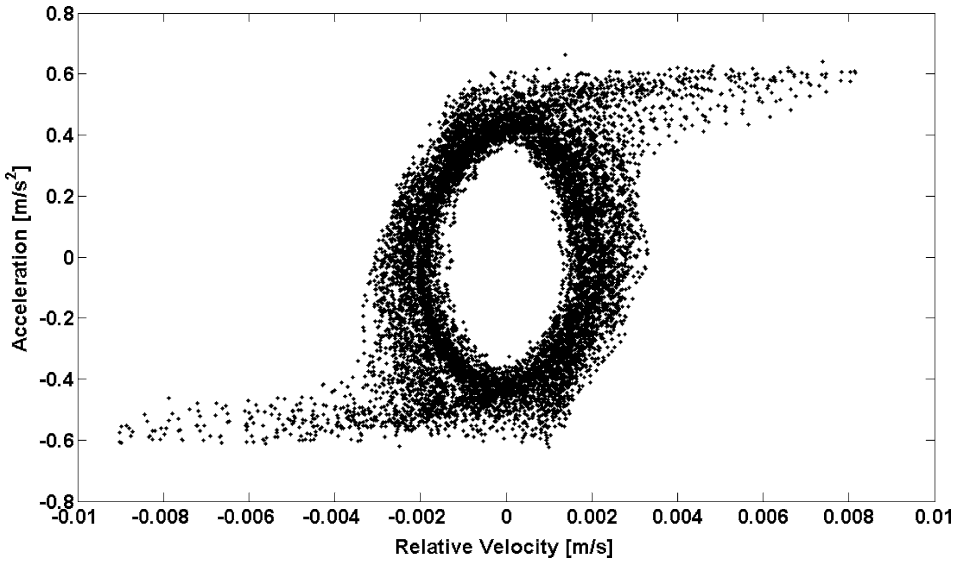

Fig. 2 Nonlinear shock damping showing saturation at a certain relative clearance velocity (frequency 4.12 Hz)

measurements to make in experimental data analysis and can also be integrated to estimate velocity and displacement time histories; therefore, restoring force methods are especially appropriate for experimental purposes. Note, however, that the static (DC) components of the velocity and displacement time histories are lost in the integration process; consequently, certain types of nonlinearities such as quadratic stiffness nonlinearities, which produce steady streaming (i.e., a DC response), may be difficult to characterize.

2.2 Frequency domain nonlinear ARX models

The models, based on discrete frequency models (DFMs) developed in [14] and applied in [19, 20], take the form

$$Y(k) = B(k)U(k) + \sum_{r,s \in \Re_i} A_{r,s}(k) \times f_{r,s}\left(Y\left(\frac{p_r}{q_r}k\right), Y\left(\frac{p_s}{q_s}k\right)\right) \quad (2)$$

where k, r, s, $(p_r/q_r)k$, and $(p_s/q_s)k$ are contained in the set of real integers, $\Re_i$, k is a simple frequency counter (i.e. $\omega = k\Delta\omega$), $U(k)$ is the input, and $B(k)$ and $A_{r,s}(k)$ are complex frequency coefficients. The first term, the exogenous component, accounts for the nominal linear dynamics and the second term, the autoregressive (AR) component, accounts for the nonlinear frequency correlations. The rational number arguments, $(p_r/q_r)k$, are used to represent different harmonics of the excitation frequency. As stated earlier, Equation (2) indicates that the harmonic response of a nonlinear system at each frequency is correlated with both the input and response at potentially all the harmonics of the input frequency. This multidimensional correlation is due to nonlinear feedback in the system.

The linear forms of the functions $f_{r,s}(\cdot)$ indicate in what frequency ranges the nonlinear correlations exist but may not describe all of the nonlinear dependencies of the response on the input. On the other hand, when the $f_{r,s}(\cdot)$ are nonlinear functions of the harmonics of the spectrum, $Y(k)$, then the model can more fully describe different types of nonlinear behavior. In summary, the $f_{r,s}(\cdot)$ determine the degree to which the frequency domain ARX model is able to describe the behavior of the nonlinear system.

These models use frequency spectra of measured signals and spectra are easier to obtain from signals with broad frequency content; therefore, experimental application of this technique is suited to broad-band inputs (e.g., random).

Equation (2) can be written as,

$$Y(k) = Dp \quad (3)$$

where p are the exogenous and auto-regressive coefficients and D contains the input and the terms $f_{r,s}(\cdot)$. The optimum set of ARX coefficients, the ones that minimize the sum of the squared error, $e(k) \cdot e(k)$, is given by the pseudo-inverse solution, $\widehat{p}$, to the over-determined Equation (3):

$$\widehat{p} = D^{+}Y(k) = (D^{T}D)^{-1}D^{T}Y(k) \tag{4}$$

where D^{+} is the pseudo-inverse of D and D^{T} is the transpose.

The order of the nonlinear ARX model is determined by the number of auto-regressive (AR) terms that are included in the function $f_{r,s}(\cdot)$, on one side of the frequency of interest, ω_k. Two forms of the ARX model are used in this paper.

First Order, Linear:

$$Y(k) = B(k)U(k) + \sum_{j=-1\neq 0}^{1} A_j(k)Y(k-j) \tag{5}$$

where, only correlations with one frequency above and one frequency below the input frequency are considered.

First Order, Nonlinear:

$$Y(k) = B(k)U(k) + A_{-1}(k)Y^3\left(\frac{k}{3}\right) + A_1(k)Y^3(3k) \tag{6}$$

where, correlations with the cubic sub- and super-harmonics are considered.

The changes in the auto-regressive coefficients (related to nonlinear behavior) can be used as indicators of damage, as damage often causes changes in the linear/nonlinear behavior of a structural system. A number of other indicators can be used that signify the onset and progression of damage in a system. The indicators used in this paper are $A_j\,(k)$, the auto-regressive coefficients, and $1 - \left|A_{j_d}/A_{j_{un}}\right|$, where '*d*' indicates damaged and '*un*' indicates undamaged. $1 - \left|A_{j_d}/A_{j_{un}}\right|$ indicate the change in the nonlinear correlations compared to the undamaged case.

2.2.1 Damage location

Equation (2) can easily be adapted for passive data (output-only) by using the transmissibility function formulation, where a measured output at a location different than that for $Y(k)$ is used as the input term, $U(k)$. Johnson and Adams [22] showed that transmissibility functions could be used to effectively detect and locate structural changes. Transmissibility functions only contain the zeros, and not the poles, of discrete frequency response functions (FRF), and therefore, contain information about more localized regions of structures. For example, a two degree-of-freedom system has an FRF matrix

$$\mathbf{H}(\omega) = \frac{1}{\Delta(\omega)}\begin{bmatrix} B_{11}(\omega) & B_{12}(\omega) \\ B_{21}(\omega) & B_{22}(\omega) \end{bmatrix} \tag{7}$$

where $\Delta(\omega)$ is the characteristic polynomial whose roots are the system poles. The entries $B_{ij}(\omega)$ contain the system zeros, which are a function of a few of the total degrees of freedom in the system. Transmissibility is defined as the ratio of two response degrees of freedom. The following equation shows that the characteristic polynomial is cancelled in the transmissibility calculation, and all that remains is the ratio of system zeros:

$$\begin{aligned} T_{ij(k)}(\omega) &= \frac{X_{ik}(\omega)}{X_{jk}(\omega)} = \frac{\frac{X_i(\omega)}{F_k(\omega)}}{\frac{X_j(\omega)}{F_k(\omega)}} \\ &= \frac{H_{ik}(\omega)}{H_{jk}(\omega)} = \frac{\frac{B_{ik}(\omega)}{\Delta(\omega)}}{\frac{B_{jk}(\omega)}{\Delta(\omega)}} = \frac{B_{ik}(\omega)}{B_{jk}(\omega)} \end{aligned} \tag{8}$$

Thus, acceleration response measurements can be used to directly access information about the zeros of the system FRFs. This property means that a transmissibility measurement across two discrete structural degrees of freedom will primarily contain information about the structural path between those two degrees of freedom. Damage and other structural changes can hence be detected and located within a sensor array.

3 Experimental setups

Laboratory experiments were performed on a full-vehicle two-post shaker test rig and a vehicle corner test rig with different damage mechanisms as described below.

3.1 Full-vehicle tests

Response data were taken on the front left suspension system of an Isuzu Impulse using a hydraulic shaker apparatus. A picture of the experimental setup is shown in Fig. 3. The MTS® hydraulic shakers, with a maximum dynamic pressure of 3000 psi, an input frequency range of 0–100 Hz and a maximum stroke of approximately 8 in., were used to excite the front left and right tire patch of the car in the vertical direction. Tri-axial accelerometers of nominal sensitivity 1 V/g were attached at five locations on the suspension system, (a) bottom of the strut, $\ddot{x}_1(t)$ (unsprung mass), (b) the upper strut connection with the body, $\ddot{x}_2(t)$, (sprung mass) (c) steering knuckle-control arm connection, $\ddot{x}_3(t)$, (d) control arm, $\ddot{x}_4(t)$ and (e) sway bar, $\ddot{x}_5(t)$. It should be noted that the actual system has more DOF than the model in Fig. 1. Damage was introduced in the suspension system of the Isuzu by loosening the bolt connecting the steering knuckle to the control arm, through a ball joint.

3.2 Vehicle corner tests

The setup consisted of a Dodge Dakota shock module, steering knuckle, lower and upper control arms and tie rod (Fig. 4). A vertical input was applied to the steering knuckle through a MTS® hydraulic shaker. Tri-axial acceleration measurements were made at the clevis joint (where the shock module attaches to the lower control arm), $\ddot{x}_1(t)$, top shock mount, $\ddot{x}_2(t)$, and the input location, $\ddot{x}_3(t)$. The vertical, longitudinal and lateral loads at the top shock mount were also available, and they were utilized as in $F_2 = M_2\ddot{x}_2$. Damage was introduced by making a cut in one of the clevis ears.

Fig. 3 Full-vehicle shaker test setup

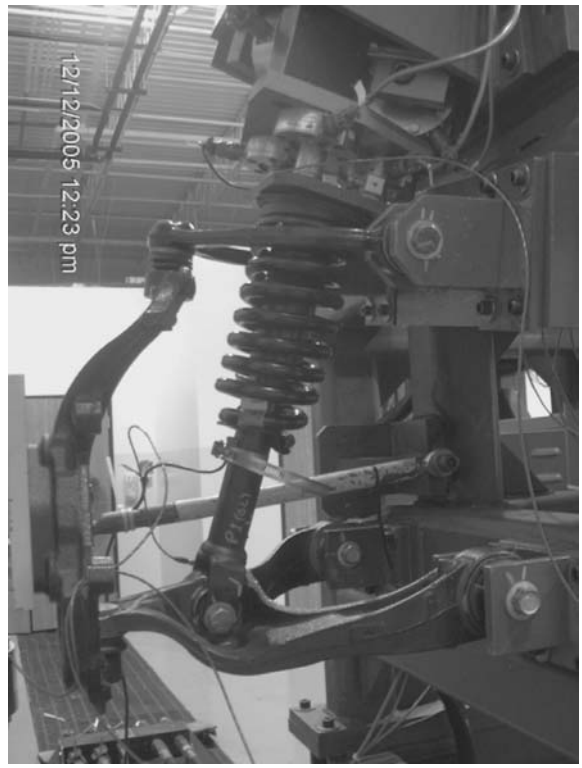

Fig. 4 Vehicle corner test rig

Sine sweep inputs were used to generate the restoring forces and broad-band random inputs were used for the ARX models. The acceleration signals were recorded with an Iotech® portable data acquisition system converted into '.mat' files and integrated offline in MATLAB® to estimate the velocity and displacement responses. The Iotech® system allowed a wide range of sampling frequencies and the application of high and/or low pass filters to remove noise and aliasing. The signal processing parameters are given in Tables 1 and 2.

Table 1 Signal processing parameters for sine sweep input

Test	Chirp range (Hz)	Chirp rate (Hz/s)	Number of time points, N_t	Sampling frequency, F_s (Hz)	Low pass filter (LPF) cut-off (Hz)
Full-vehicle	0–15	0.025	360,000	600	100
Vehicle corner	0–35	0.058	360,000	600	100

Table 2 Signal processing parameters for random input

Test	Time points, N_t	Frequency content (Hz)	Sampling freq., F_s (Hz)	Number of averages, N_{avg}	Overlap (%)	LPF cut-off (Hz)
Full-vehicle	180,000	0–35	600	100	50	100
Vehicle corner	168,000	0–20	600	100	50	100

4 Damage detection

4.1 Bolt loosening

Damage was introduced in the suspension system of the ISUZU by loosening the bolt connecting the steering knuckle to the control arm, through a ball joint (Fig. 5), from an initial torque of 400 in-lb to 250 in-lb, then 100 in-lb and finally removing the bolt completely. Self-loosening is often a problem in bolted joints, especially in joints under cyclic transverse loading [23]. This has great importance in automotive applications since the fasteners generally represent the largest single cause of warranty claims faced by automobile manufacturers [24].

Fig. 5 Bolt damage location

4.1.1 Restoring forces

In order to characterize the nonlinear internal loads of the suspension system, the quarter car model of Fig. 1 was used to generate velocity (damping) and displacement (stiffness) restoring force curves, for the undamaged case. Figure 2 shows a representative restoring force curve, in the vertical direction between the top strut mount ($\ddot{x}_2(t)$), and the steering knuckle-control arm connection ($\ddot{x}_3(t)$), for an input amplitude of 0.5 mm. It shows the top strut mount acceleration versus the velocity difference between the top mount and the steering-knuckle control arm connection. The restoring force curve shows a nonlinear damping characteristic with both saturation (Coulomb friction damping curve) and hysteresis. Figures 6 and 7 show the frequency characteristics of the damping and stiffness restoring forces between the top mount and the steering-knuckle control arm connection. The damping force initially has a central hysteresis loop, but as the frequency increases the force takes on the shape of a Coulomb friction curve, then a piecewise-linear characteristic and finally it becomes primarily linear with some hysteresis. The stiffness force shows primarily hysteresis with backlash at certain frequencies.

The same restoring force curves were generated for the different damage cases to study the change in the nonlinear internal forces with progression of damage. Figures 8 and 9 show the change in the frequency characteristics of the damping and stiffness restoring forces with the progressive loosening of the bolt. The intermediate cases (loosened bolts, 250 in-lb (. . .), 100 in-lb (- - -)) show a change in the nonlinear characteristics at higher frequencies (the frequency at which the restoring

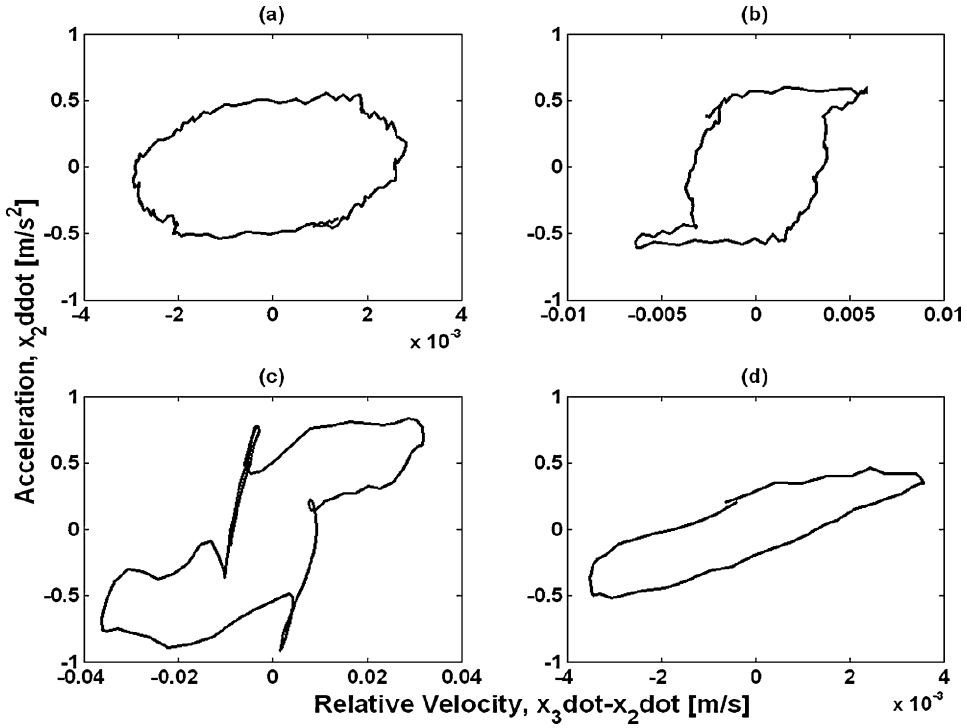

Fig. 6 Frequency characteristic of damping internal force in the strut (**a**) 4.05 Hz, (**b**) 4.17 Hz, (**c**) 6.67 Hz and (**d**) 12.5 Hz

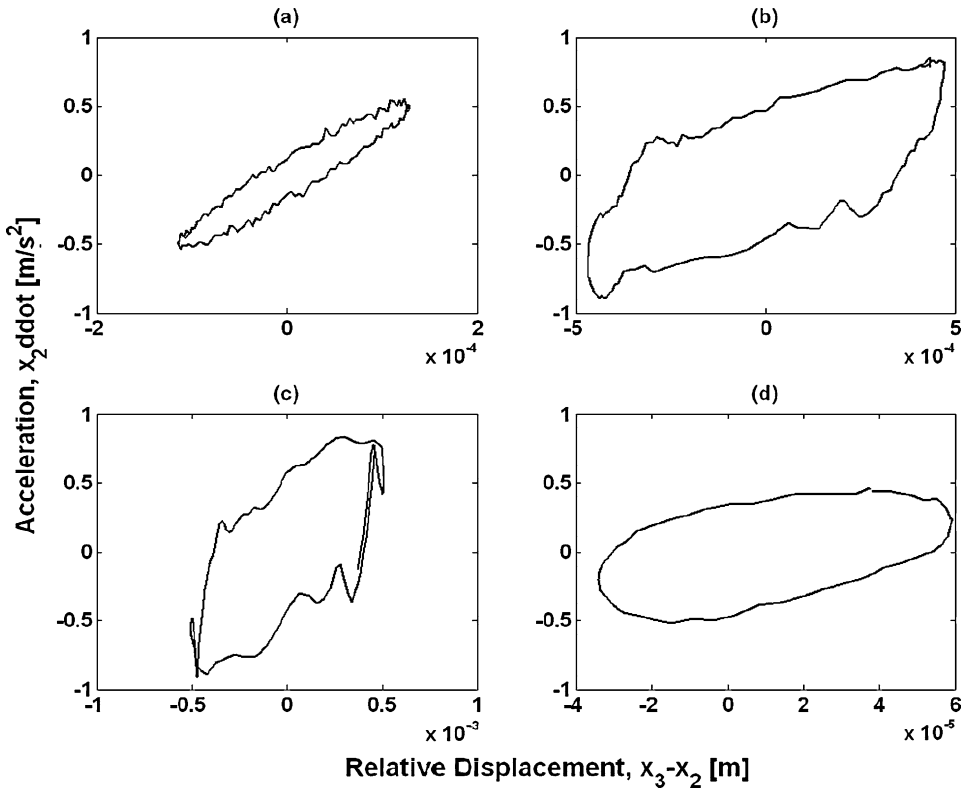

Fig. 7 Frequency characteristic of vertical stiffness internal force in the strut (**a**) 4.05 Hz, (**b**) 4.5 Hz, (**c**) 6.67 Hz and (**d**) 12.5 Hz

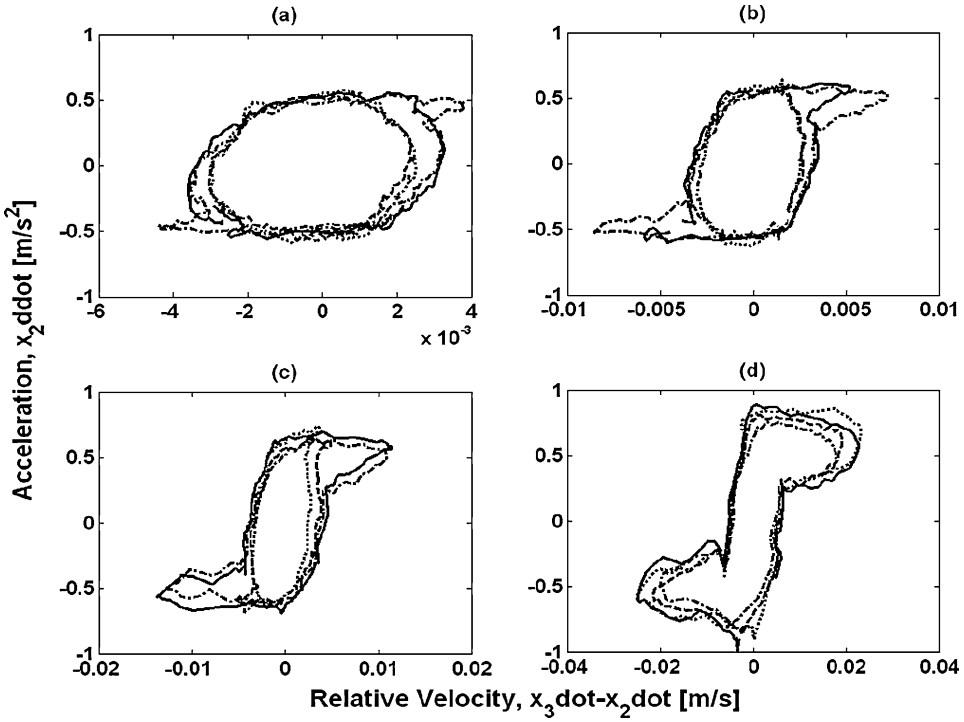

Fig. 8 Change in frequency characteristic of vertical damping internal force in the strut with damage. Bolt torques: Undamaged, 400 in-lb (——), 250 in-lb (· · ·), 100 in-lb (– – –) and no bolt (– .–. –). Frequency: (**a**) 4.09 Hz, (**b**) 4.17 Hz, (**c**) 4.26 Hz and (**d**) 4.67 Hz

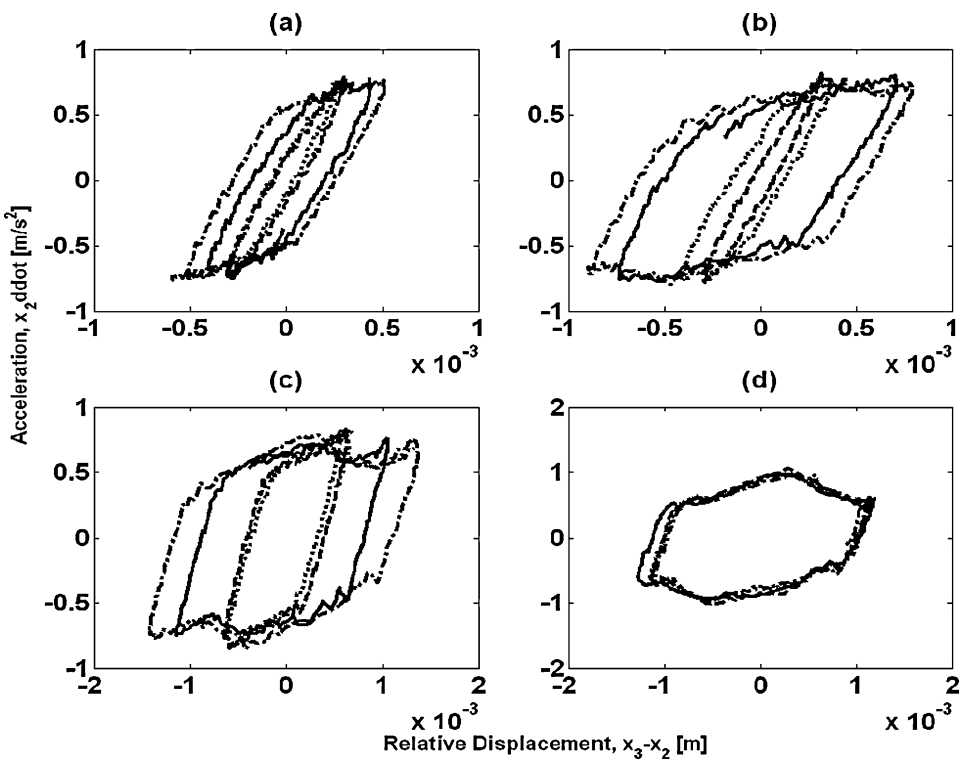

Fig. 9 Change in frequency characteristic of vertical stiffness internal force in the strut with damage. Bolt torques: Undamaged, 400 in-lb (——), 250 in-lb (· · ·), 100 in-lb (– – –) and no bolt (– .–. –). Frequency: (**a**) 2.66 Hz, (**b**) 2.71 Hz, (**c**) 2.75 Hz and (**d**) 3.16 Hz

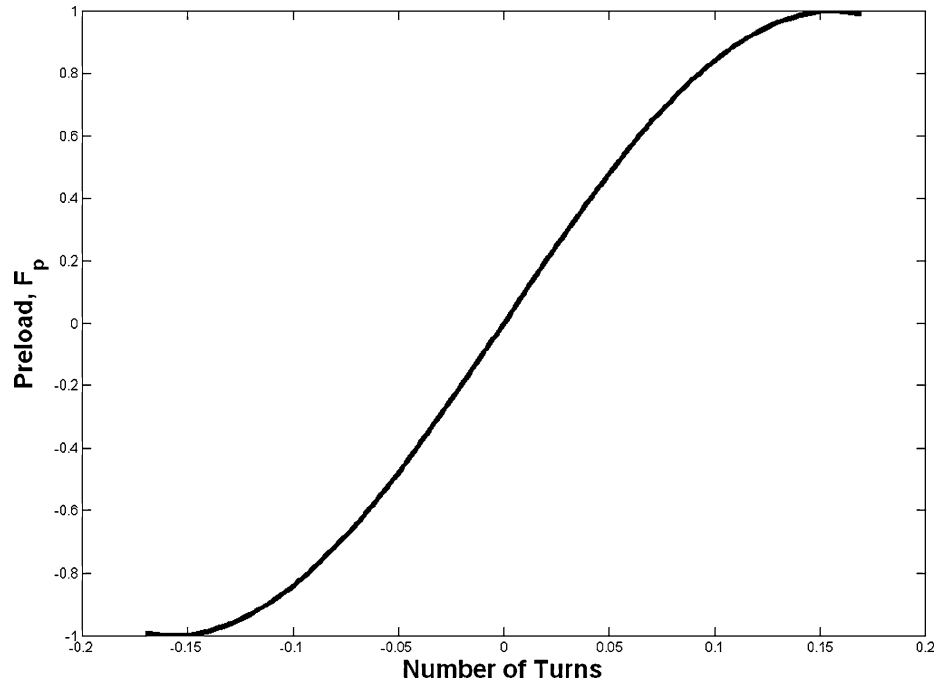

Fig. 10 Bolt preload as a function of the number of turns

force corresponding to 100 lb-in bolt torque changes is the highest) compared to the undamaged case, and the most severe damage case (bolt removed) changes characteristic at a lower frequency than the undamaged case. For example, in Fig. 8a at 4.09 Hz, the damping restoring force corresponding to the case with no bolt has already taken on the shape of a Coulomb friction curve while the restoring forces for the other three cases only show a hysteresis loop. The undamaged restoring force assumes the Coulomb friction form at a later frequency of 4.17 Hz and the loosened bolt cases do not begin to take this form until 4.26 Hz. This same behavior is observed for different input amplitudes. The stiffness restoring force also exhibits a change in frequency behavior. In Fig. 9a (2.66 Hz) the undamaged case and the case with no bolt show backlash while the loose bolt cases show primarily linearity with some hysterisis. Significant backlash does not appear for the loose bolt cases until 2.75 Hz (Fig. 9c). Damage has caused a fundamental change in the frequency behavior of the internal nonlinear loads. As the frequency characteristics of the damping internal load changes to the appearance of a Coulomb friction damping load, it seems that the loosened bolt restricts the relative velocity, and increases friction, which causes the system to stay in the central hysteresis loop longer in terms of frequency. On the other hand, the lack of a bolt allows greater relative velocity and the characteristic of the force changes at a lower frequency.

The restoring force curves also show that once the damping restoring force curves have become piecewise linear and the stiffness restoring forces exhibit backlash for all cases, there is a difference in the areas of the curves (Figs. 8d and 9d). It is clearer for the damping load in Fig. 8d where there is a decrease in area as the bolt is loosened. This decrease in area signifies a decrease in the internal load. This is the case for the damping and stiffness restoring forces for all frequencies beyond the initial range where the changes in the characteristics occur.

To understand these results the mechanism of bolted joints must be considered. As a nut is rotated on a bolt's screw thread against a joint, the bolt is extended. This extension generates a tension force or bolt preload. The reaction to this force is a clamp force that causes the joint to be compressed. The number of turns of the bolt affects the preload and the typical preload versus turn behavior is shown in Fig. 10. Equation (9) relates the bolt preload to the turn angle [24]:

$$F_p = \theta \left(\frac{p}{360}\right)\left(\frac{K_{\text{bolt}} K_j}{K_{\text{bolt}} + K_j}\right) \tag{9}$$

where p is the thread pitch, K_{bolt} is the bolt stiffness, and K_j is the joint material stiffness. The equation shows that as the bolt is loosened, the preload decreases, which results in a decrease in the clamp force on the joint. Thus, the internal load between the lower ball joint and the top mount decreases as the bolt is loosened and is the lowest when the bolt is removed completely. This accounts for the decrease in the area of the restoring force curves with loosening of the bolt (Fig. 8d).

It should be noted that in generating the restoring force curves using the acceleration rather than the force of a component the resulting plots are scaled by the component mass, M. It is also assumed that the mass remains constant throughout, which may not be the case. Therefore, it is possible that changes in effective mass due to degrees of freedom acting between measurements taken across a damaged component are partially responsible for the observed changes in the restoring force curves. For example, the path between the lower ball joint and the top strut mount has a mode of vibration between 4 and 5 Hz. A change in mass would cause the frequency of this mode to change, which could in turn affect the frequency characteristics of the restoring forces.

4.1.2 Frequency domain nonlinear ARX models

The models were applied using random input data with a Gaussian distribution for various input amplitudes ranging from 0.5 to 6.0 mm RMS displacements of the wheel pan (i.e., tire patch of the Isuzu).

First, the first-order, linear model in Equation (5) was applied to the data from points which had the damage location in their path, and the damage features were estimated. Figure 11 shows the estimated damage feature $1 - |A_{j_d}/A_{j_{un}}|$ for the vertical motion data from points x_2 and x_3, with x_3 taken as the input, $U(k)$.

Figure 11 shows the quantity $1 - |A_{j_d}/A_{j_{un}}|$ for $A_1(k)$. Any nonzero value shows a change in the autoregressive coefficients and is an indicator of change in nonlinearity. There is an obvious change in the 40–55 Hz range where the 100 lb-in torque case exhibits more nonlinear correlation than the other cases. It can be seen that the 250 lb-in torque case does not introduce any significant changes in the nonlinear correlations, and the undamaged case and the case with no bolt have very similar behavior. The coefficients $A_{-1}(k)$ show the same trends. Figure 12 shows a typical self-loosening sequence of a bolted joint due to transverse cyclic loading [23]. The symbol P represents the clamping force,

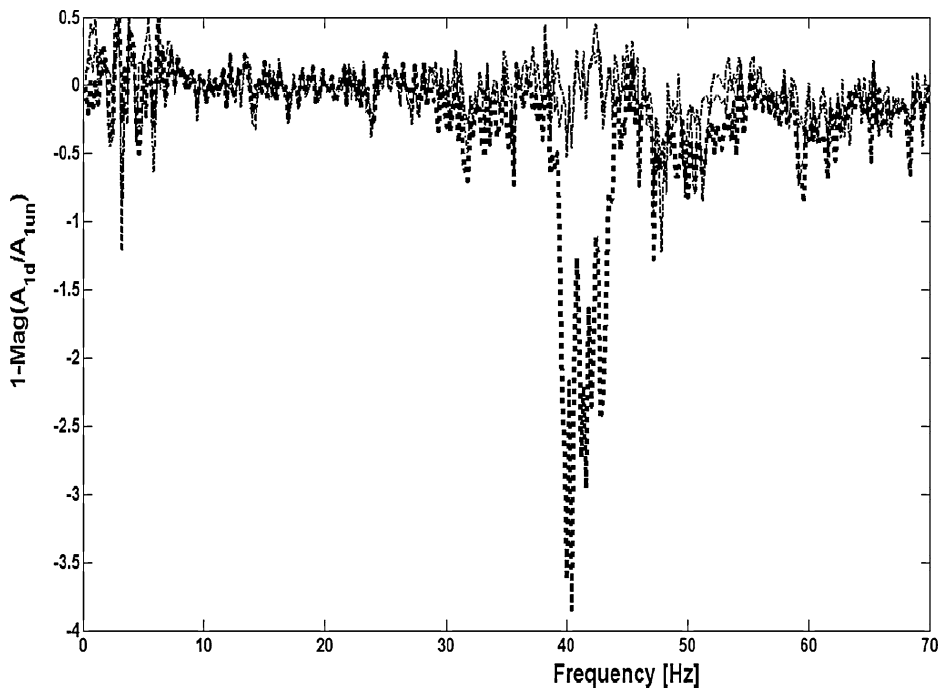

Fig. 11 1-Mag($A_{1d}(\omega)/A_{1un}(\omega)$) for first-order linear model (vertical direction); 250 lb-in torque (– – –), 100 lb-in torque (· · ·) and no bolt (–.–.–)

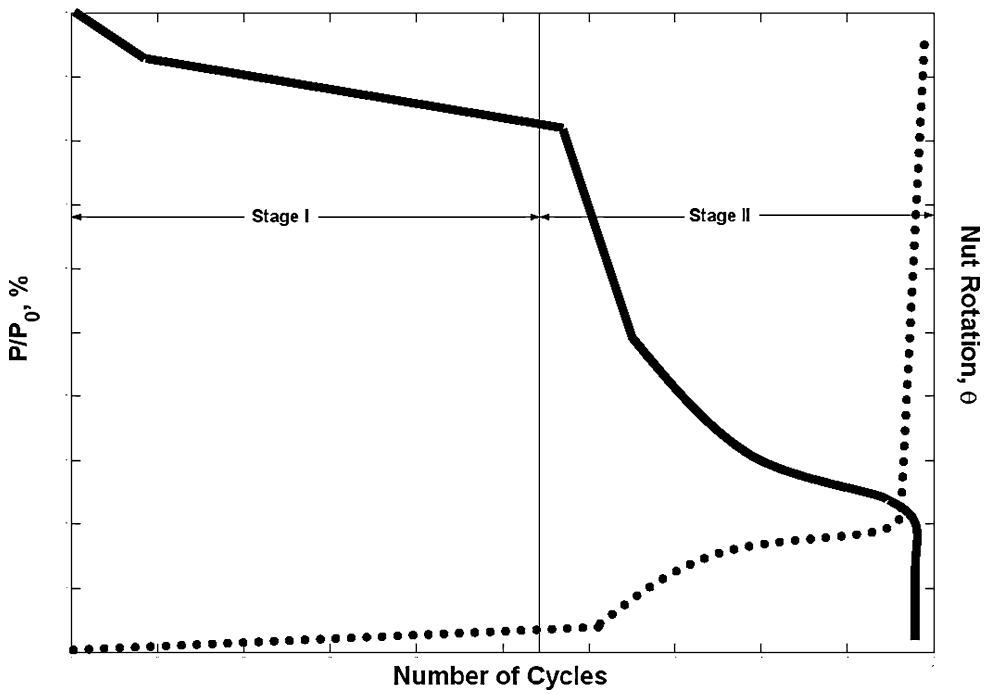

Fig. 12 Self-loosening sequence of a bolted joint due to transverse cyclic loading; percentage preload loss (——), nut rotation (degrees) (· · ·). (Jiang et al. [23] – reprinted with the permission of ASME)

P_0 represents the initial clamping force or preload, and θ is the rotation angle of the nut against the bolt. This figure is relevant as the loading on the ball joint bolt in the suspension system of the vehicle under investigation is primarily transverse. Two distinct stages can be identified in the figure. During the first stage, there is very little relative motion between the nut and the bolt. The later stage is characterized by backing-off of the nut and rapid loosening of the clamping force with relative motion between the bolt and the joint. The second of the two loose bolt conditions (100 lb-in torque) that is simulated in the experiments belongs to the second stage. These stages of bolt loosening suggest that there is a critical value of the preload at the junction of the two stages seen in Fig. 12 where relative motion occurs at the joint and nonlinear correlations increase. The indicators discussed show that as the bolt is loosened, the nonlinearity in the path between x_2 and x_3 increases, due to the increased friction between the bolt and the ball joint caused by relative motion (Hess et al. [25, 26], showed that loosening and relative motion can occur in the presence of vibration). This friction force is governed by the equation for friction between surfaces in contact, Equation (10):

$$F_f = \mu N \tag{10}$$

where μ is the coefficient of friction (static or kinetic) and N is the normal load between the joint threads. When the bolt is completely loosened or actually removed from the joint the normal load goes to zero as there is no contact load and this source of friction force is no longer active, resulting in the nonlinearity in the path between the two measurement locations returning to the original undamaged level.

The increase in friction due to the relative motion between the bolt and the joined components results in an increase in the nonlinear frequency correlations seen in Fig. 11. On the other hand, the removal of the source of increased friction (namely, the bolt) results in the nonlinear correlations returning to the undamaged levels. This behavior is similar to the behavior observed in the restoring forces. The intermediate damage cases have different characteristics from the undamaged case and the most severe case (no bolt) behaves similar to the undamaged case.

The lateral direction data exhibits the same pattern but to a lesser extent than the vertical direction, as shown in Fig. 13, which is on the same scale as the vertical case. The longitudinal direction indicator (Fig. 14) shows the least change. In fact, it is almost insignificant compared to the other two cases. The cause of this is that the bolt axis is in the longitudinal direction.

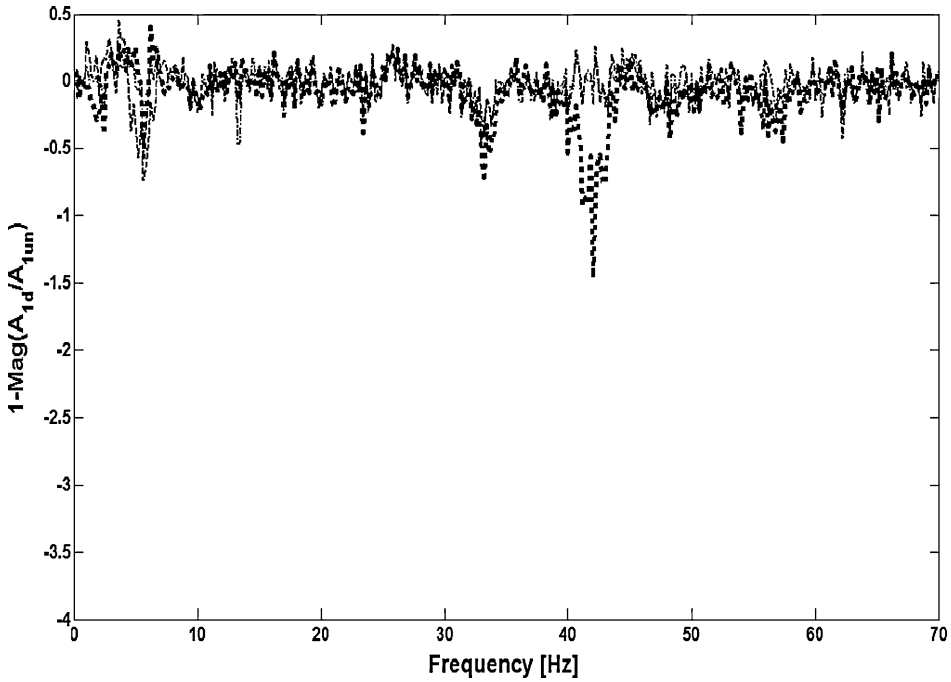

Fig. 13 1-Mag($A_{1d}(\omega)/A_{1un}(\omega)$) for first-order linear model (lateral direction); 250 lb-in torque (– – –), 100 lb-in torque (· · ·) and no bolt (–.–.–)

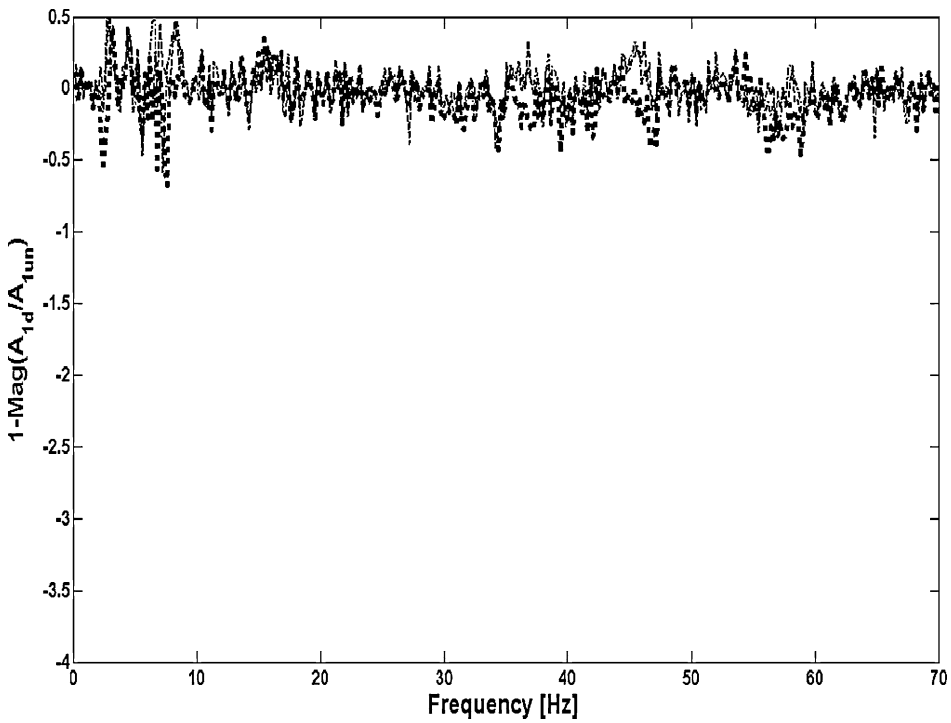

Fig. 14 1-Mag($A_{1d}(\omega)/A_{1un}(\omega)$) for first-order linear model (longitudinal direction); 250 lb-in torque (– – –), 100 lb-in torque (· · ·) and no bolt (–.–.–)

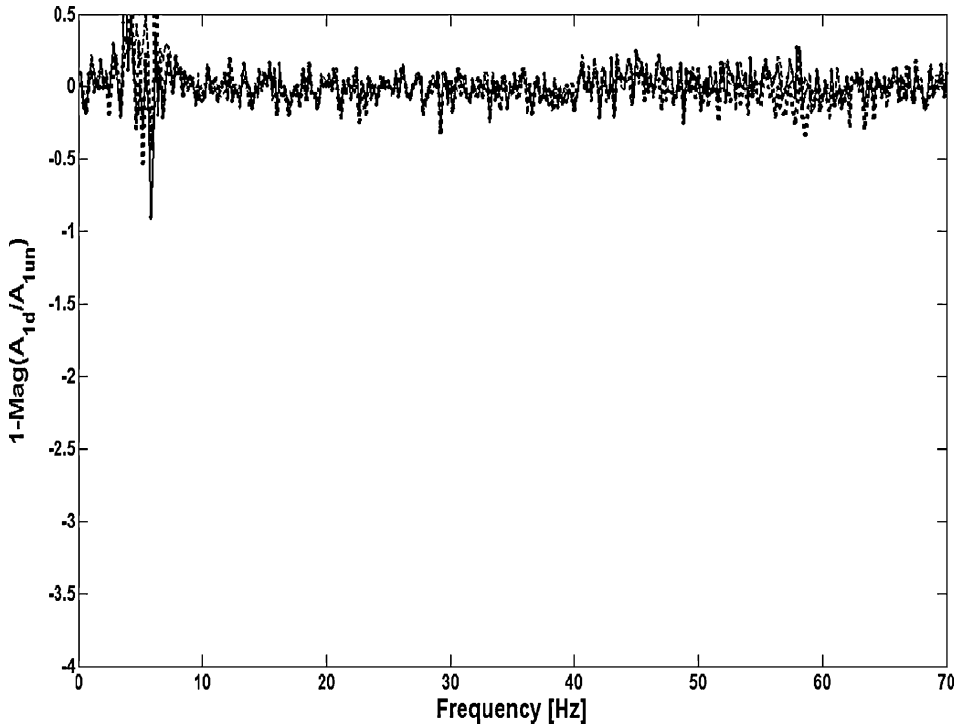

Fig. 15 1-Mag($A_{1d}(\omega)/A_{1un}(\omega)$) for first-order linear model applied to points with no damage in their path (vertical direction); 250 lb-in torque (– – –), 100 lb-in torque (· · ·) and no bolt (–.–.–)

Loosening of the bolt causes motion about the longitudinal axis (motion along the longitudinal axis is restricted because the bolt still applies some clamping force); hence, the vertical and lateral directions show greater changes in nonlinear correlations. So, the axis of the bolt can also be identified.

As explained earlier, the output-only formulation of the nonlinear ARX models allows the damage to be located due to increased sensitivity to changes in local dynamics. To verify this, the first-order linear model was applied to data from locations which did not have the damage in their path. Figure 15 shows the estimated indicator $1 - \left|A_{j_d}/A_{j_{un}}\right|$ for the data from points on the control arm and the sway bar. It is clear that there are no significant changes in the nonlinear correlations in the path between these two points. Hence, the damage has been located.

A first-order nonlinear model was also applied to the data. A cubic form of the nonlinear model (Equation (6)) was chosen as opposed to a quadratic form because the Coulomb friction nonlinearity changes with the loosening of the joint as discussed earlier. This discontinuous nonlinearity can be approximated with odd polynomial functions (i.e., x^3, x^5, etc.). In addition, symmetric nonlinearities (Figs. 6 and 7) tend to result in odd harmonics. It was observed that although there were significant quadratic harmonic correlations, they did not show any significant changes with damage because the damage primarily affects Coulomb friction. The same trends as before were observed (Fig. 16), with the nonlinear correlations increasing for the 100 lb-in case and decreasing when the bolt is removed. In fact, the 100 lb-in torque case shifts the nonlinear correlation with the third super-harmonic (Fig. 16b) of the input excitation at about 7.5 to 8 Hz. The autoregressive coefficients also show an interesting result; the super-harmonic frequency correlations are much stronger than the sub-harmonic correlations. This result suggests that the nonlinear feedback due to the third super-harmonic of the forced response of the system (which is symptomatic of nonlinear behavior) is much greater than the sub-harmonic. In the nonlinear model we are assuming than the nonlinearity is cubic in nature, hence, if the forcing function is harmonic (e.g., $\cos(\omega t)$) the cube of the function gives frequency components at the forcing frequency and the third multiple.

$$(\cos(\omega t))^3 = \frac{3}{4}\cos(\omega t) + \frac{1}{4}\cos(3\omega t) \tag{11}$$

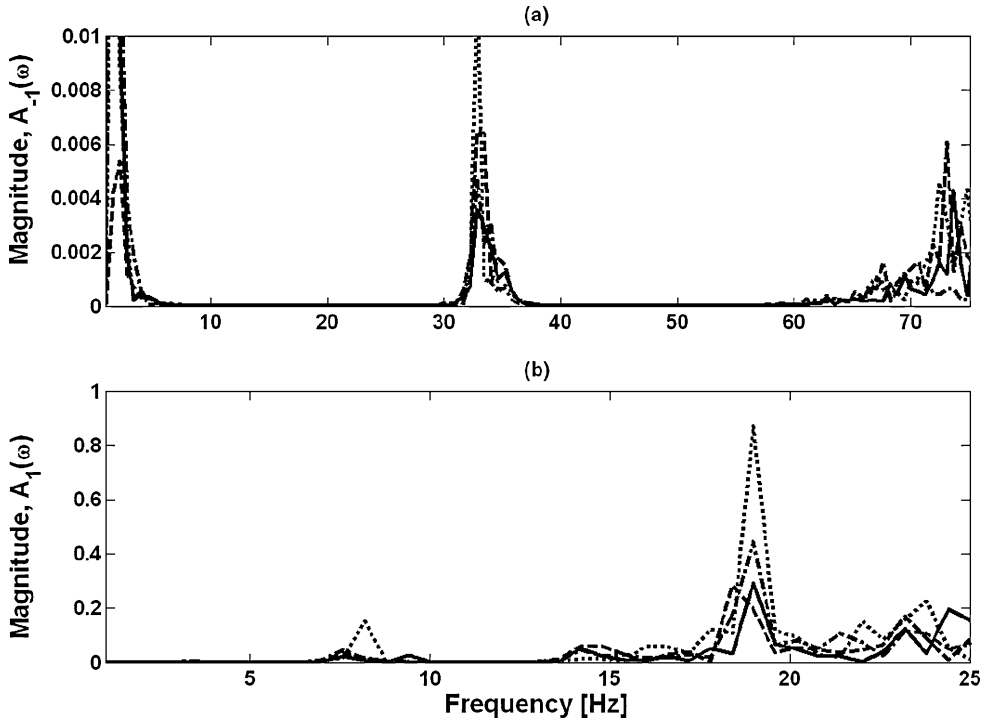

Fig. 16 Auto-regressive coefficients $A_{-1}(\omega)$ (sub-harmonic) and $A_1(\omega)$ (super-harmonic) for first order nonlinear model; coefficients for undamaged case, 400 lb-in (—-), and damaged cases, 250 lb-in (– – –), 100 lb-in (· · ·) and no bolt (–.–.–)

Equation (11) shows that there are no sub-multiple components. The super-harmonic correlations interact with the forced response components at other excitation frequencies to produce sub-harmonic correlations via frequency combinations. The resulting sub-harmonic correlations are weaker in this case. The response of the system is primarily forced because the data was collected for a broad-band input after the system had reached steady-state., i.e. the system transients had died out.

4.2 Cut in a member

Damage was introduced in a Dodge Dakota suspension sub-system by making a cut in a coil-over-shock-module clevis ear as shown in Fig. 17. Similar damage has been observed by automotive suspensions components suppliers during durability testing of coil-over-shock modules. The system was run through a durability schedule using vehicle operating test files supplied by the OEM.

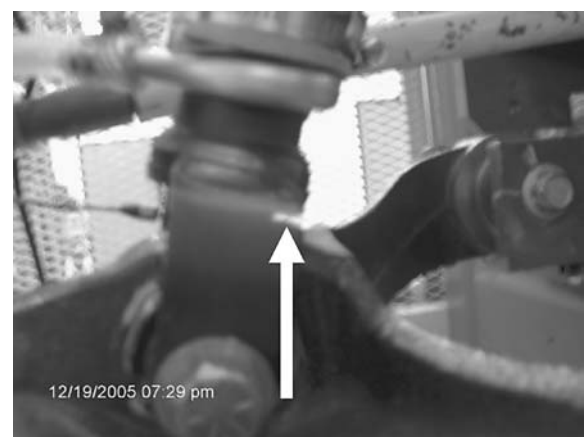

Fig. 17 Initial cut in shock clevis

4.2.1 Restoring forces

As before, sine sweep (0.058 Hz/s) input data was collected at regular intervals to generate the restoring forces. Figure 18 shows the frequency characteristics of the damping internal force along the axis of the shock. The damping force changes from piecewise linear at

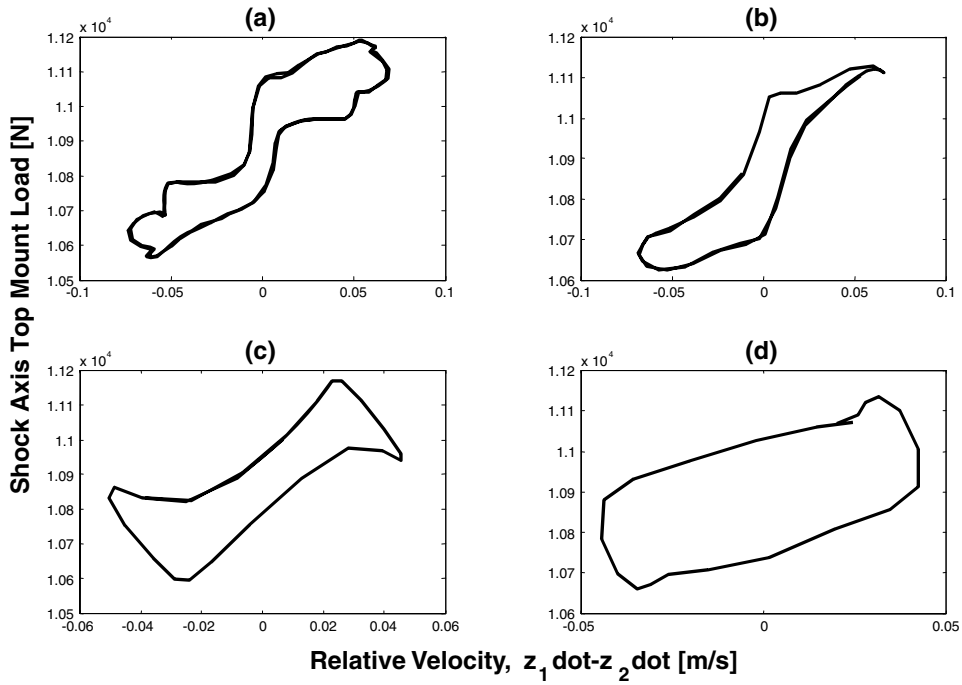

Fig. 18 Frequency characteristic of vertical damping internal force along the axis of the shock module (**a**) 7.8 Hz, (**b**) 19.5 Hz, (**c**) 27.2 Hz and (**d**) 29.2 Hz

lower frequencies to primarily hysteretic at higher frequencies.

Figure 19 shows the change in the internal damping force with the initial damage. There is a reduction in the internal load with a change in slope signifying an increase in the damping. Two undamaged restoring forces are presented to show that the change with damage is greater than the variability from test to test. Durability tests were run for two days with the system shut-off over night. Figure 20 shows the change in the internal force with usage due to damage at the end of the first day of testing and the change after the system has been allowed to rest. As the test progresses, the damping internal force not only decreases but the nonlinear characteristic also changes. This change can be attributed to the crack-like behavior of the cut, where it 'breathes' as the cyclic load is applied. It is interesting to note that the area of the restoring force curve and, thus, the internal load actually increases after the system has been allowed to rest. The reason for this is that when testing is stopped for a significant amount of time, the load in the members redistributes and it is redirected when the testing resumes. Figure 20 also shows that when the system is allowed to rest there is a permanent change in the internal force. In this case, there is an increase in the amount of damping as the slope increases. It will be shown later that although usage also causes a change in the internal loading, the redistribution of the internal loads after external load is removed results in the same amount of loading as before external load is applied. At the end of the durability tests, the clevis ear was cut through completely (Fig. 21). Figure 22 shows how this affects the internal damping force. This causes a decrease in the internal force and an increase in the damping as the area decreases and the slope increases. Damage has changed the magnitude and nonlinear characteristic of the internal damping force of the shock module. The reason that the change is not more dramatic for the complete cut is that the clevis collapses onto the ear and contact is maintained. Hence, it only results in a change in the amount of internal force.

Change in internal loads with usage. In order to study the effect of usage on the internal loads of components and verify that damage causes a permanent change in the internal loads full-vehicle tests were run on the 2-post shaker setup. Sweep data was collected at the

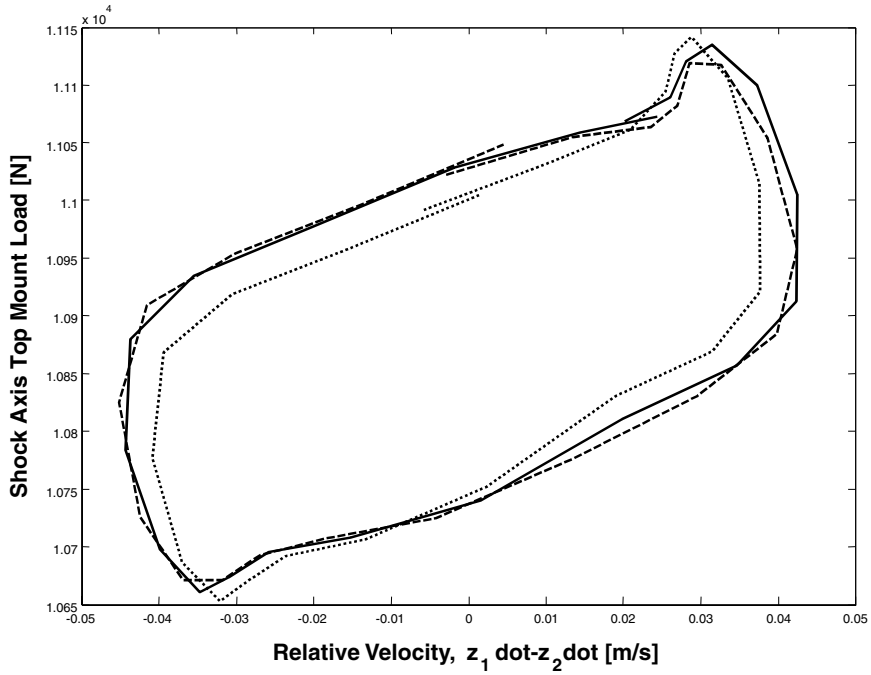

Fig. 19 Change in internal damping force of the shock module with initial damage (29.2 Hz); baseline 1 (——), baseline 2 (– – –) and initial cut (· · ·)

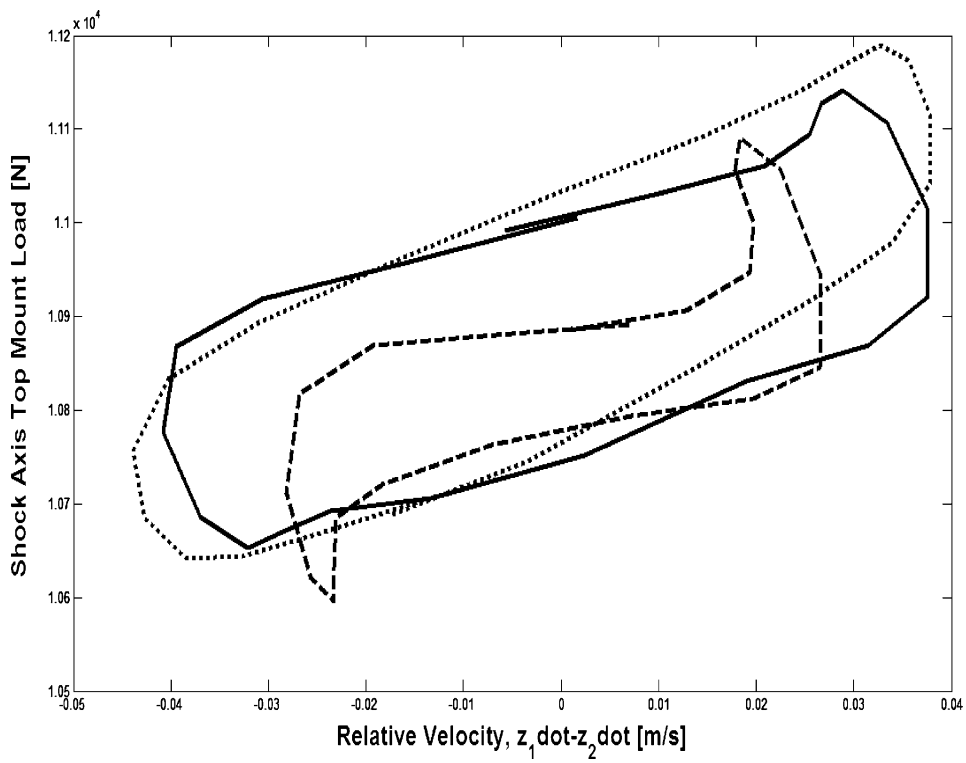

Fig. 20 Change in internal damping force of the shock module with damage (29.2 Hz); Initial damage (——), progressed damage (– – –) and permanent change after rest (· · ·)

Fig. 21 Complete cut in shock clevis

beginning and then high amplitude broadband input tests were run continuously for 10 h. Data was collected at the end of the tests and again after the vehicle sat idle for 24 h. Figure 23 shows the change in the vertical damping internal load of the sway bar link along with the variation from baseline to baseline. The internal load increases with usage but returns very close to the initial state upon removal of the external load(s). The differences between the final load and the baseline are comparable to the variation from baseline to baseline. It is clear from this result and the results from the previous damage scenario that the internal loads change with both usage and damage, but the change due to damage is permanent. When the external load is removed, the internal loads are redistributed resulting in a change in the restoring force area, but some residual load remains because of the presence of damage. Similar behavior is seen for other locations in the suspension system. Thus, the permanent change in the internal loads is an indicator of the level of damage.

4.2.2 Frequency domain nonlinear ARX models

The linear and nonlinear models were applied using random inputs, with a frequency content of 0–20 Hz, to the steering knuckle.

First, the first-order, linear model in Equation (5) was applied to the data from points which had the damage location in their path, and the complex coefficients were estimated. Figure 24 shows the estimated autoregressive coefficient, $A_1(k)$, for the vertical motion

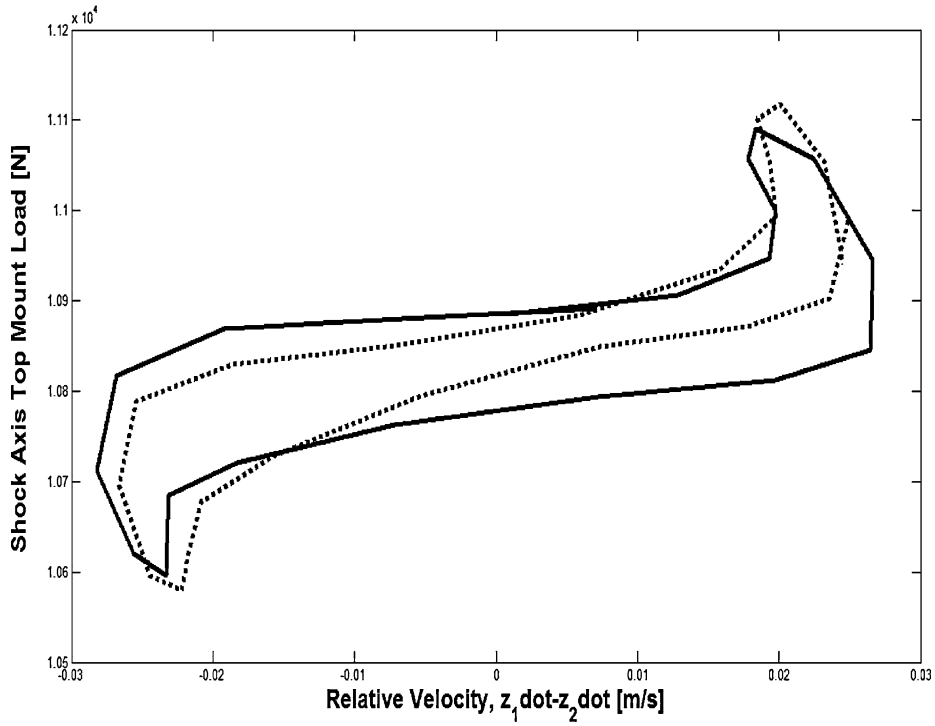

Fig. 22 Change in internal damping force of the shock module with damage (29.2 Hz); progressed damage with 1/4 cut (——), and complete cut (· · ·)

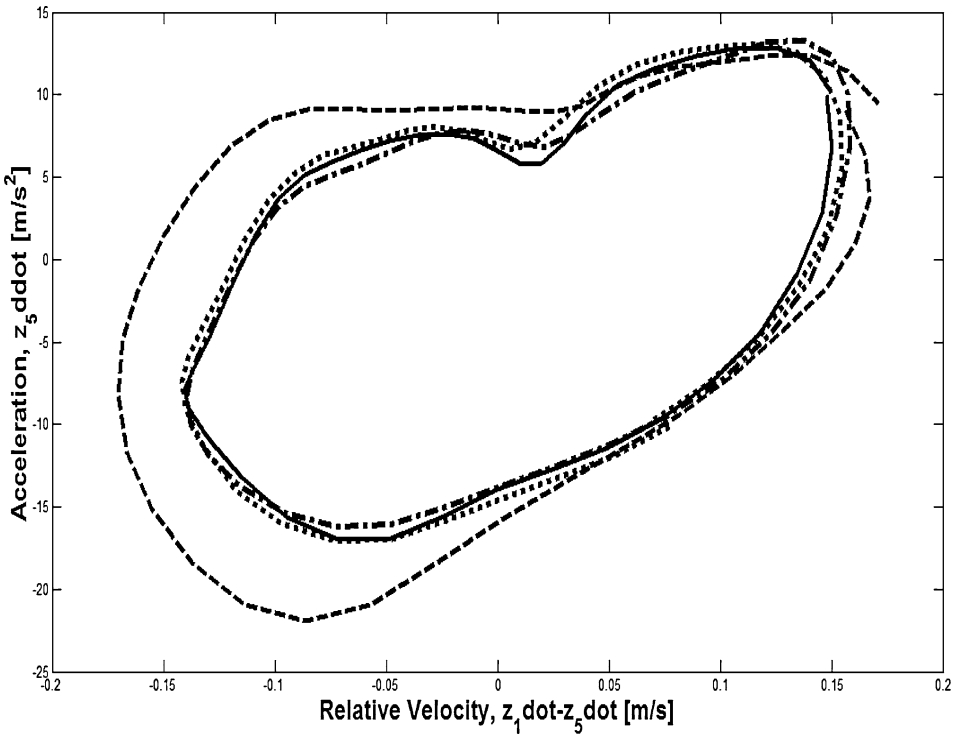

Fig. 23 Change in internal damping force of the sway bar link with usage (34 Hz); Baseline 1 (——), baseline 2 (– .–. –), after 10 h of testing (– – –) and after 24 h of idle time (· · ·)

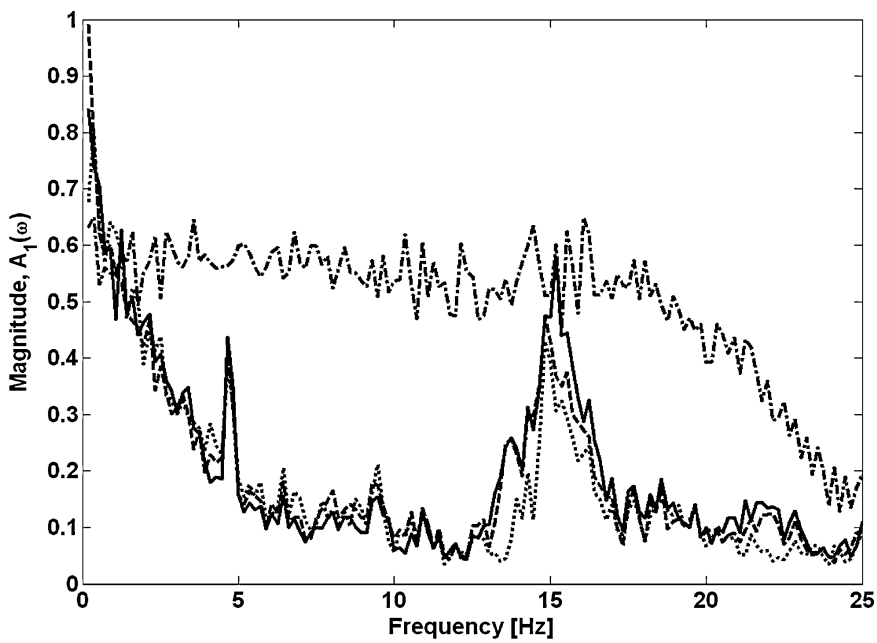

Fig. 24 Vertical direction auto-regressive coefficients for first order linear model (clevis damage); coefficients for undamaged case (—-), initial cut (– – –), progressed damage Day 1 (· · ·) and final cut (–.–.–)

data from points x_1 and x_2, with x_1 taken as the input, $U(k)$.

Figure 24 shows the change in the nonlinear correlations with the initial damage, the progressed damage at the end of the first day of durability testing and after the final cut. It is clear that correlations with the next highest frequency decrease as the damage is introduced and then grows. The clearest indication is around

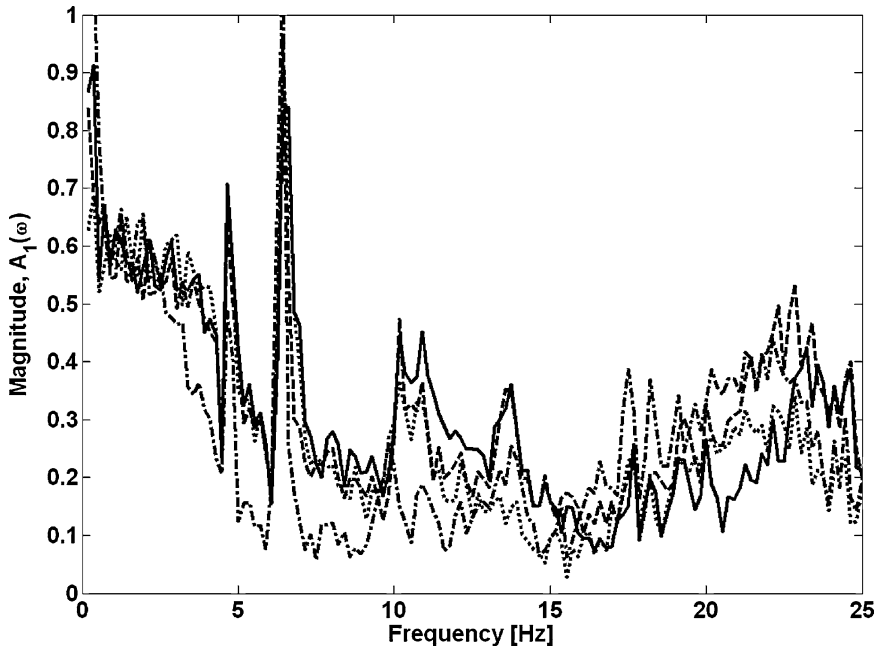

Fig. 25 Longitudinal direction auto-regressive coefficients for first-order linear model (clevis damage); coefficients for undamaged case (——), initial cut (– – –), progressed damage Day 1 (· · ·) and final cut (–.–.–)

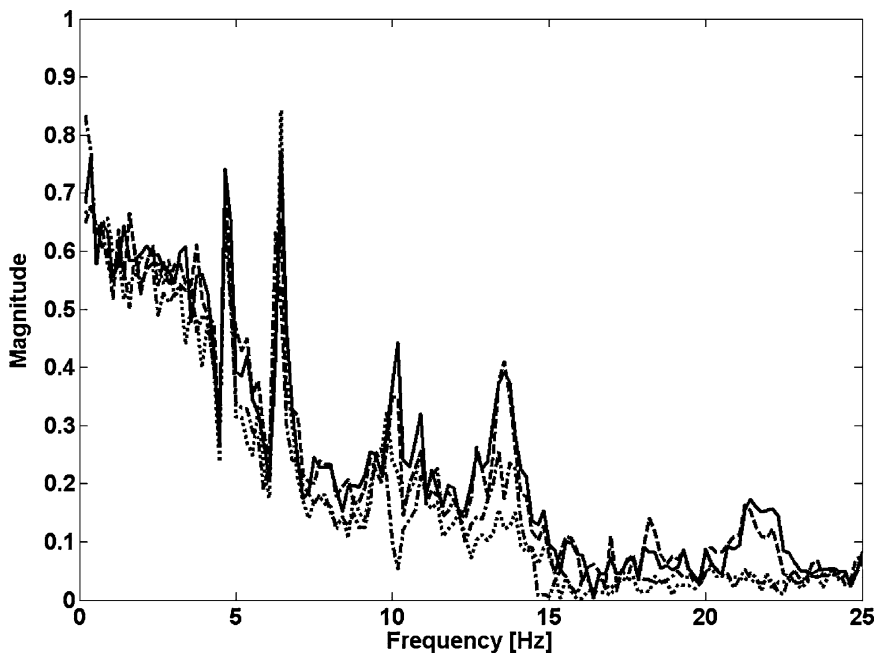

Fig. 26 Lateral direction auto-regressive coefficients for first order linear model (clevis damage); coefficients for undamaged case (——), initial cut (– – –), progressed damage Day 1 (· · ·) and final cut (–.–.–)

15 Hz. The changes in the nonlinear correlations with the final cut are more dramatic compared to the change in the internal loads. The final cut actually causes the nonlinear correlations to increase significantly across the entire frequency range, because although contact is maintained there is relative motion due to the cyclic loading. Thus, the changes in the nonlinear frequency correlations provide a better indication of the effect of complete failure of the clevis.

The longitudinal direction data (Fig. 25) shows that the nonlinear correlations decrease with damage below 15 Hz. In this direction, the final cut causes the correlations to decrease further rather than increasing. Another difference is that the nonlinear frequency correlations

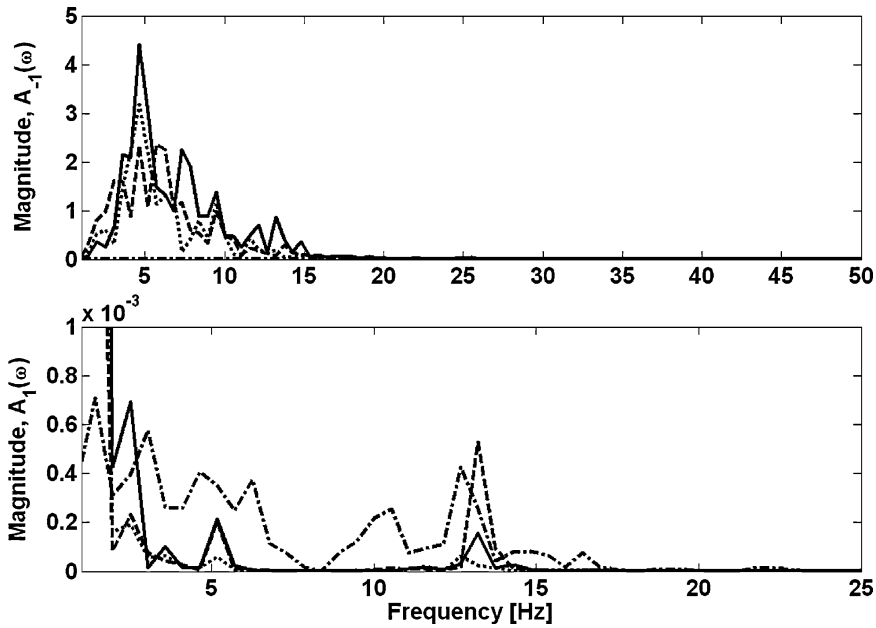

Fig. 27 Vertical direction auto-regressive coefficients $A_{-1}(\omega)$ (sub-harmonic) and $A_1(\omega)$ (super-harmonic) for first-order nonlinear model; coefficients for undamaged case (——), initial cut (– – –), progressed damage Day 1 (· · ·) and final cut (–.–.–)

actually increase in the 15–23 Hz range, and are highest for the final cut. The lateral direction (Fig. 26) shows a similar pattern to the longitudinal direction with no dramatic increase in the nonlinear correlations with the final cut.

The reason that only the vertical direction indicators show a dramatic increase in nonlinear frequency correlations with the final cut is that the motion of the shock module is primarily along that direction, and the clevis and the clevis ear maintain contact even after the complete cut. Consequently, there is significant rattling as the system vibrates, leading to an increase in the nonlinear behavior. There is slipping between the surfaces in the longitudinal and lateral directions, but the relative motion is restricted by the rigidity of the components. The increase in nonlinear correlations due to friction is only apparent in the higher frequency range for the longitudinal direction. The differing changes for the three directions provide information about the direction of the cut in the clevis.

The cubic form of the first-order, nonlinear model (Equation (6)) was also applied to the data for this damage scenario. In this case, the quadratic harmonic correlations were not only significant but also showed changes with damage because the restoring force curves have significant asymmetry (Figs. 19, 20 and 22), which changes with damage (Fig. 20). However, only the results of the cubic model are discussed here. The vertical direction coefficients (Fig. 27) show that, unlike the bolt damage case, the sub-harmonic correlations (Fig. 27a) are much stronger than the super-harmonic correlations (Fig. 27b). In this case, the system nonlinearities result in super-harmonic correlations interacting with the forced response components at other excitation frequencies to produce stronger sub-harmonic correlations via frequency combinations. The same trends as the linear model are observed, with the super-harmonic correlations increasing significantly with the final cut, but the sub-harmonic correlations actually become almost zero. The longitudinal and lateral directions show the same trends as the linear model and also have stronger sub-harmonic correlations than super-harmonic correlations.

5 Conclusions

It was shown that methods which characterize the nonlinear nature of mechanical systems can be used to detect and locate nonlinear mechanical damage. Restoring forces (time domain) were used to detect changes in the nonlinear internal forces and frequency domain nonlinear ARX models were used to track changes in the nonlinear frequency correlations with the progress of different damage mechanisms introduced in automotive suspension systems. An important feature of these methods is that an input measurement is not required; measurements of output accelerations suffice.

In fact, it was shown that only using the outputs in the ARX models allows damage to be located due to the increased sensitivity to local dynamics of the system.

Acknowledgements The authors would like to thank ArvinMeritor and the Purdue University Center for Advanced Manufacturing for their financial support of this research.

References

1. Siebert, W.M.: Signals and Systems. McGraw Hill, New York (1986)
2. Bracewell, R.N.: The Fourier Transform and its Applications, 2nd edn. WCB/McGraw-Hill, Boston, MA (1986)
3. Thrane, N.: The Hilbert Transform. Hewlett Packard Application Notes (1984)
4. Chui, C.K.: An Introduction to Wavelets. Academic Press, San Diego, CA (1992)
5. Leontaritis, I., Billings, S.A.: Input–output parametric models for non-linear systems. Part I: Deterministic non-linear systems. Int. J. Control **41**(2), 303–328 (1985)
6. Storer, D.M., Tomlinson, G.R.: Recent developments in the measurement and interpretation of higher order transfer functions from non-linear structures. Mech. Syst. Signal Process. **7**(2), 173–189 (1993)
7. Collis, W.B., White, P.R., Hammond, J.K.: Higher-order spectra: the bispectrum and trispectrum. Mech. Syst. Signal Process. **12**, 375–394 (1998)
8. Surace, C., Worden, K., Tomlinson, G.R.: On the nonlinear characteristics of automotive shock absorbers. Proc. Inst. Mech. Eng.: Part D **206**(D1), 3–16 (1992)
9. Audenino, A.L., Belingardi, G.: Modeling the dynamic behavior of a motorcycle damper. J. Automobile Eng.: Part D **209**, 249–262 (1995)
10. Haroon, M., Adams, D.E., Luk, Y.W., Ferri, A.A.: A time and frequency domain approach for identifying non-linear mechanical system models in the absence of an input measurement. J. Sound Vib. **283**, 1137–1155 (2005)
11. Haroon, M., Adams, D.E., Luk, Y.W.: A technique for estimating linear parameters using nonlinear restoring force extraction in the absence of an input measurement. ASME J. Vib. Acoustics **127**(5), 483–492 (2005)
12. McGee, C.G., Haroon, M., Adams, D.E.: A frequency domain technique for characterizing nonlinearities in a tire-vehicle suspension system. ASME J. Vib. Acoustics **127**(1), 61–76 (2005)
13. Adams, D.E., Allemang, R.J.: Residual frequency autocorrelation as an indicator of nonlinearity. Int. J. Non-Linear Mech. **36**, 1197–1211 (2000)
14. Adams, D.E., Allemang, R.J.: Discrete frequency models: a new approach to temporal analysis. ASME J. Vib. Acoustics **123**(1), 98–103 (2001)
15. Masri, S.F., Caughey, T.K.: A nonparametric identification technique for nonlinear dynamic problems. J. Appl. Mech. **46**, 433–447 (1979)
16. Masri, S.F., Sassi, H., Caughey, T.K.: Nonparametric identification of nearly arbitrary nonlinear systems. J. Appl. Mech. **49**, 619–628 (1982)
17. Masri, S.F., Miller, R.K., Saud, A.F., Caughey, T.K.: Identification of nonlinear vibrating structures: Part I – Formulation. J. Appl. Mech. **54**, 918–922 (1987)
18. Masri, S.F., Miller, R.K., Saud, A.F., Caughey, T.K.: Identification of nonlinear vibrating structures: Part II – Applications. J. Appl. Mech. **54**, 923–930 (1987)
19. Adams, D.E.: Frequency domain ARX model and multi-harmonic FRF estimators for non-linear dynamic systems. J. Sound Vib. **250**(5), 935–950 (2002)
20. Adams, D.E., Farrar, C.R.: Classifying linear and non-linear structural damage using frequency domain ARX models. Struct. Health Monit. **1**(2), 185–201 (2002)
21. Zhang, H., Schulz, M.J., Naser, A., Ferguson, F., Pai, P.F.: Structural health monitoring using transmittance functions. Mech. Syst. Signal Proc. **13**(5), 765–787 (1999)
22. Johnson, T.J., Adams, D.E.: Transmissibility as a differential indicator of structural damage. ASME J. Vib. Acoustics **124**(4), 634–641 (2002)
23. Jiang, Y., Zhang, M., Lee, C.H.: A study of early stage self-loosening of bolted joints. ASME J. Mech. Des. **125**, 518–526 (2003)
24. Bickford, J.H.: An Introduction to the Design and Behavior of Bolted Joints. Marcel Dekker, New York (1990)
25. Hess, D.P., Davis, K.: Threaded components under axial harmonic vibration, Part I: Experiments. ASME J. Vib. Acoustics **118**(3), 417–422 (1996)
26. Hess, D.P., Sudhirkashyap, S.V.: Dynamic loosening and tightening of a single-bolt assembly. ASME J. Vib. Acoustics **119**, 311–316 (1997)